6p photoionization in high-Z elements and the influences of relativistic Cooper minima

S. T. Manson and C. J. Lee

Department of Physics and Astronomy, Georgia State University, Atlanta, Georgia 30303

R. H. Pratt and I. B. Goldberg*

Department of Physics and Astronomy, University of Pittsburgh, Pittsburgh, Pennsylvania 15260

B. R. Tambe

Department of Chemistry and Physics, Southern Technical Institute, Marietta, Georgia 30060

Akiva Ron

Racah Institute of Physics, Hebrew University of Jerusalem, Jerusalem 91904, Irasel

(Received 8 March 1983)

Relativistic Dirac-Slater calculations of the photoionization of the 6p subshell in elements in the range $82 \leq Z \leq 100$ have been performed, examining cross sections, branching ratios, and angular distributions. The zero (Cooper minimum) which appears in the $6p \rightarrow \epsilon d$ nonrelativistic matrix element is split into three relativistically, for the matrix elements $6p_{3/2} \rightarrow \epsilon d_{3/2}$, $6p_{3/2} \rightarrow \epsilon d_{5/2}$, and $6p_{1/2} \rightarrow \epsilon d_{3/2}$. The outstanding feature of our results is the huge energy splitting between these minima, more than an order of magnitude larger than the discrete $6p_{3/2}$-$6p_{1/2}$ splitting. The origin of this phenomenon is discussed along with its consequences for angular distributions and branching ratios.

I. INTRODUCTION

During the past two decades, the overall systematics of photoionization of low-Z atoms has become largely understood through the continued interplay of theory and experiment.[1-4] However, the calculations of the process, at various levels of approximation, have been predominantly nonrelativistic. Thus their ability to deal with high-Z systems (where relativistic effects are of importance and experimental work is sparse) is not well known. We have, therefore, embarked upon a project of calculation of various aspects of the photoionization process for heavy atoms over a wide range of subshells, within an explicitly relativistic framework. Our main effort is toward elucidating the effects due specifically to relativistic interactions and how these effects depend upon atomic number Z. To this end, we compare calculations made nonrelativistically, based on the Schrödinger equation, and relativistically, based on the Dirac equation, using the same atomic model in each case.

One of the features of the photoionization process which is most sensitive to the details of the interaction, and on which we therefore focus in the present work, is the so-called Cooper minimum[5,6] (or, perhaps, Dichtburn-Bates-Seaton-Cooper minima), characterized by a photon energy for which the dipole matrix element in the dominant $l \rightarrow l+1$ channel has a zero. These minima occur extensively in photoionization of outer and near-outer subshells; we have chosen to study the 6p subshell initially. In this case the single nonrelativistic p-d matrix element splits relativistically into three matrix elements,

$p_{1/2} \rightarrow d_{3/2}$, $p_{3/2} \rightarrow d_{3/2}$, and $p_{3/2} \rightarrow d_{5/2}$; each has its own Cooper minimum (zero) at a different position and some recent preliminary work has shown that the splittings in energy of the positions of these three zeros are much larger than originally anticipated.[7] To understand the situation more fully, we present herein a more systematic study of the energy dependence of 6p photionization matrix elements for $82 \leq Z \leq 100$. The cross sections, branching ratios, and angular distribution asymmetry parameters are also examined to identify the observable consequences of the splittings and relativistic motion of these minima.

In the next section we give a brief review of the calculational methodology and the atomic potentials employed. Section III presents and discusses our results. Section IV gives a summary and a prospectus for future work.

II. THEORY AND METHOD OF CALCULATION

In the central field approximation, the relativistic cross section for photoionization of an electron in an (n,l,j) subshell of an atom by electric dipole radiation (a fairly good approximation for $h\nu \lesssim 500$ eV) is given, in atomic units and jj coupling, by[8]

$$\sigma = \frac{4\pi c}{\omega k} \left[\frac{N_{nlj}}{2j+1} \right] \left[\frac{2j-1}{12j} |R_{j-1}|^2 + \frac{1}{12j(j+1)} |R_j|^2 \right. $$

$$\left. + \frac{2j+3}{12(j+1)} |R_{j+1}|^2 \right], \qquad (1)$$

where ω is the photon energy, the photoelectron momentum $k = [(E+c^2)(E-c^2)/c^2]^{1/2}$, with E ($> m_0c^2$) the total energy of the ejected photoelectron, N_{nlj} is the occupation numer of the subshell, and the R_j are the (complex) single-particle radial matrix elements corresponding to transitions into final continuum states of angular momentum j. The continuum functions are normalized such that the asymptotic amplitudes of the large and small components are $[(E \pm c^2)/(2E)]^{1/2}$, respectively; this corresponds to unit amplitude in the nonrelativistic limit. We can write $R_j = \bar{R}_j e^{i\xi_j}$ where $\bar{R}_j$ is real and ξ_j is the sum of the Coulomb phase shift ξ_C and the non-Coulomb phase shift δ_j. The details are given elswhere.[9,10] In the cases of $p_{1/2}$ and $p_{3/2}$ electrons, Eq. (1) reduces to

$$\sigma = \frac{4\pi c}{\omega k}\left(\frac{1}{9}\mid R_{s_{1/2}}\mid^2 + \frac{2}{9}\mid R_{d_{3/2}}\mid^2\right) \qquad (2)$$

and

$$\sigma = \frac{4\pi c}{\omega k}\left(\frac{1}{9}\mid R_{s_{1/2}}\mid^2 + \frac{1}{45}\mid R_{d_{3/2}}\mid^2 + \frac{1}{5}\mid R_{d_{5/2}}\mid^2\right) , \qquad (3)$$

respectively.

The angular distribution of photoelectrons produced in an electric dipole process is given by[11,12]

$$\frac{d\sigma}{d\Omega} = \frac{\sigma}{4\pi}[1 + \beta P_2(\cos\theta)] , \qquad (4)$$

where σ is the total cross section, P_2 is the Legendre polynomial $[P_2(x) = (3x^2 - 1)/2]$, θ is the angle betweeen photoelectron direction and the photon polarization, and β is the asymmetry parameter. The same form of expression is also applicable for unpolarized photons if now θ is the angle between photon and photoelectron directions and the replacement $\beta \rightarrow \beta/2$ is made.[13]

The expression for the asymmetry parameter β in j-j coupling in the central field approximation is[8]

$$\beta = \left[\frac{(2j-3)(2j-1)}{48j^2}\mid R_{j-1}\mid^2 - \frac{(2j-1)(2j+3)}{48j^2(j+1)^2}\mid R_j\mid^2 + \frac{(2j+3)(2j+5)}{48(j+1)^2}\mid R_{j+1}\mid^2 \right.$$

$$\left. + \frac{(2j-1)}{8j^2(j+1)}[\text{Re}(R_jR_{j-1}^*)] + \frac{(2j+3)}{8j(j+1)^2}[\text{Re}(R_jR_{j+1}^*)] + \frac{(2j-1)(2j+3)}{8j(j+1)}[\text{Re}(R_{j-1}R_{j+1}^*)] \right]$$

$$\times \left[\frac{(2j-1)}{12j}\mid R_{j-1}\mid^2 + \frac{1}{12j(j+1)}\mid R_j\mid^2 + \frac{(2j+3)}{12(j+1)}\mid R_{j+1}\mid^2 \right]^{-1} . \qquad (5)$$

In the cases of $p_{1/2}$ and $p_{3/2}$ electrons, Eq. (5) reduces to

$$\beta_{p_{1/2}} = \frac{2\bar{R}_{d_{3/2}}^2 + 4\bar{R}_{s_{1/2}}\bar{R}_{d_{3/2}}\cos(\xi_{s_{1/2}} - \xi_{d_{3/2}})}{\bar{R}_{s_{1/2}}^2 + 2\bar{R}_{d_{3/2}}^2} \qquad (6)$$

and

$$\beta_{p_{3/2}} = [36\bar{R}_{d_{5/2}}^2 - 4\bar{R}_{d_{3/2}}^2 + 18\bar{R}_{d_{3/2}}\bar{R}_{d_{5/2}}\cos(\xi_{d_{3/2}} - \xi_{d_{5/2}}) + 10\bar{R}_{s_{1/2}}\bar{R}_{d_{3/2}}\cos(\xi_{s_{1/2}} - \xi_{d_{3/2}})$$

$$+ 90\bar{R}_{s_{1/2}}\bar{R}_{d_{5/2}}\cos(\xi_{s_{1/2}} - \xi_{d_{5/2}})](25\bar{R}_{s_{1/2}}^2 + 5\bar{R}_{d_{3/2}}^2 + 45\bar{R}_{d_{5/2}}^2)^{-1} . \qquad (7)$$

In the nonrelativistic limit where $\bar{R}_{d_{3/2}} = \bar{R}_{d_{5/2}}$, and $\xi_{d_{3/2}} = \xi_{d_{5/2}}$ Eqs. (6) and (7) are both identical to the nonrelativistic expression for β.

Central field Dirac-Slater (DS) wave functions, corresponding to pure jj coupling, were used for our calculation. The central field DS potential, along with the discrete wave functions for the initial states, was generated using the code of Lieberman et al.[14] The wave function for the final continuum orbital was generated using the same central potential in which the initial bound orbital was computed, i.e., the potential that a test charge would see in the field of a DS ground-state charge distribution, modified by a Latter tail, solving the single-particle Dirac equation using our own codes.[15,16]

One question that arises is the specification of occupation numbers of the $j = l \pm \frac{1}{2}$ spin-orbit doublets in partially filled subshells within this central field model. This is not a crucial point if the open subshell(s) is not the one be-

ing photoionized; some tests run with varying occupation numbers confirm this view. It can obviously be quite important, however, when the photoelectron comes from an open subshell, at least for predictions of the relative magnitudes of the $j = l \pm \frac{1}{2}$ cross sections. In this work, the problem arises only for the range of Z's from 81 to 85, where the $6p$ subshell is not filled. One possible choice is to assume that the lower-energy $j = l - \frac{1}{2}$ state fills first. This, however, is not consistent with the observation of both $6p_{1/2}$ and $6p_{3/2}$ electrons in the $6p^2$ subshell of lead[17] ($Z = 82$), which indicates that the "true" wave function is an admixture of $6p_{1/2}^2$ and $6p_{3/2}^2$ although the former is certainly the somewhat larger component. We have thus chosen, for simplicity, with Scofield,[18,19] to use statistical occupation numbers for open subshells, i.e., to keep the occupation numbers of the $j = l + \frac{1}{2}$ and $j = l - \frac{1}{2}$ states in the statistical ratio of $l + 1:l$ as it is in the closed subshell. In practice this leads to fractional occupation numbers.

III. RESULTS AND DISCUSSION

We have seen that the physically observable cross sections, branching ratios, and angular distributions are to be understood in terms of continuum phase shifts and transition matrix elements. Thus we will begin in the sections which follow by discussing the relativistic modifications of these quantities. This will lead us to focus on the relativistic changes in positions of Cooper minima, identifying the relativistic changes in wave functions which are responsible, and then continue with the discussion of the consequences for the physical observables.

In a relativistic treatment of the photoionization of the $6p$ subshell of heavy atoms the $6p \to \epsilon s$ and $6p \to \epsilon d$ nonrelativistic transitions split, as we have already discussed, into $6p_{3/2} \to \epsilon s_{1/2}, \epsilon d_{3/2}, \epsilon d_{5/2}$ transitions and $6p_{1/2} \to \epsilon s_{1/2}, \epsilon d_{3/2}$ transitions; the $6p_{1/2} \to \epsilon d_{5/2}$ transition is dipole forbidden since $\Delta j = 2$. Thus the two nonrelativistic dipole transitions become five when relativistic interactions are considered. In the Dirac-Slater (DS) atomic model employed in these calculations, the continuum wave function of the ejected electron is uniquely specified by its energy and angular momentum, independent of which electron of the initial state is ejected in the photoionizing transition. Thus we are dealing with only three continuum states $\epsilon s_{1/2}$, $\epsilon d_{3/2}$, and $\epsilon d_{5/2}$.

Most of our understanding of the behavior of transition matrix elements results from studies of the simpler nonrelativistic form. In what follows we will discuss the consequences of relativity in terms of this simpler formalism. Therefore, before proceeding, it is important to point out that, in addition to the calculations performed as described in the preceding section, we have done some test calculations of this nonrelativistic form using only the large components of the initial and final radial Dirac wave functions in this formalism, i.e., using the large parts of the relativistic wave functions we have done a nonrelativistic calculation. The results were quite close to those from the full relativistic matrix elements. (This would not have been true for photoionization of inner shells.) Thus we conclude that the important relativistic effects in this problem may be understood simply in terms of these large components of the discrete and continuum wave functions. This allows us to carry out the analysis of the results in the nonrelativistic manner without examining the small components of the wave functions, the relativistic dipole operator, etc.

A. Phase shifts

Since the non-Coulomb phase shifts characterize the deviations of the outer parts of the continuum wave functions with respect to Coulomb functions, important in discussing the zeros of transition matrix elements, and since they also play an important role in determining the photoelectron angular distribution asymmetry parameters, it is appropriate to begin by discussing relativistic effects on the non-Coulomb phase shift. (The relativistic effects on a Coulomb phase shift of charge $Z = 1$ are very small.) While some of these points have been noted earlier in general terms,[8] we believe a discussion focused on this particular case will be helpful.

In Fig. 1, the $\epsilon d_{5/2}$ and $\epsilon d_{3/2}$ non-Coulomb phase shifts are shown for uranium ($Z = 92$). We see that the phase-shift difference is both relatively small and roughly constant as a function of the energy. The consequence is that in Eqs. (5)—(7) the main differences in angular distributions are due to changes in $\bar{R}$, not δ. We note that the spin-orbit interaction, which splits the ϵd's, is energy independent (in contrast to, for example, the exchange interaction in a Hartree-Fock calculation, which is explicitly dependent upon the energy[20]). The phase-shift differences can be expressed in terms of an integral involving the spin-orbit Hamiltonian and the continuum wave functions.[21] The important part of the range of integration is near the nucleus where the spin-orbit force is large. In this region the continuum wave functions are virtually independent of energy over the range of energies we are considering (at very high energies this would not be true). Thus it is reasonable that the phase-shift difference is roughly energy independent. Note that $\delta_{d_{3/2}} > \delta_{d_{5/2}}$ indicating a more attractive potential for $\epsilon d_{3/2}$; this, of course, is a manifestation of the fact that the spin-orbit force is repulsive for $j = l + \frac{1}{2}$ ($\epsilon d_{5/2}$ in this case) and attractive for $j = l - \frac{1}{2}$.

These features are qualitatively the same in every case we have studied, the $\epsilon d_{3/2}$ phase shift always being greater than the $\epsilon d_{5/2}$ and their difference being nearly constant. We do however find that the difference increases with Z, as we expect, since the spin-orbit interaction increases with Z. The values of this splitting are 0.026, 0.029, 0.031, 0.034, 0.037, and 0.040 (in units of π radians) for $Z = 82, 86, 88, 92, 96$, and 100, respectively.

Also shown in Fig. 1 is the nonrelativistic d-wave phase shift for uranium obtained from a Hartree-Slater (HS) calculation.[21] This is the nonrelativistic analogy to our DS results in that each electron "sees" the field of the other electrons along with a local density approximation to exchange but within the framework of the Schrödinger equation. The relativistic and nonrelativistic non-Coulomb phase shifts can be compared directly since the low-energy Coulomb phase shifts for an electron in the field of a singly charged ion and low energies hardly differ in the two cases[22] (by an amount of order α^2). The results show that the nonrelativistic ϵd is pulled toward the nucleus as compared to either of the relativistic ϵd's and that the nonrelativistic phase shift is always greater than the relativistic; the difference, furthermore, is more or less energy independent. This indicates that the net nonrelativis-
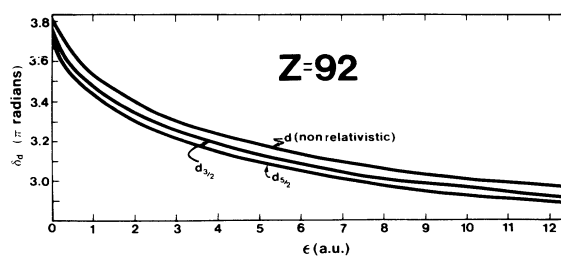

FIG. 1. d-wave phase shifts for uranium vs photoelectron energy ϵ. Relativistic $d_{3/2}$ and $d_{5/2}$ results are shown along with the nonrelativistic value.

tic potential for d waves is *more* attractive than either of the relativistic effective potentials. We observe this for all cases studied; the result is just the opposite of the hydrogenic (point Coulomb) case where all wave functions, discrete and continuum, contract under the influence of relativistic interactions.[23]

The relativistic interactions are strongest near the nucleus and get rapidly small with increasing r. Thus, for a given energy, the contraction effect is greatest for s states, whose amplitudes are greatest near the nucleus, and gets progressively smaller for p, d, and f waves, respectively, since the amplitudes decrease at small r with increasing orbital angular momentum. For multielectron atoms the extra relativistic attraction at small r is still there and all the subshells from $1s$ to $3d$ contract. However this causes the nucleus to be more screened, so that outside these subshells the net electrostatic attraction is less, relativistically, than in the nonrelativistic case. Outer subshells respond to the combination of these effects, which act in opposite directions. For the higher s and p orbitals, which have appreciable amplitude near the nucleus, the net effect is contraction, while f orbitals, which are small near the nucleus, expand. For d orbitals the two effects come closest to canceling, and the direction of the net result changes with increasing r; the $3d$ contracts and the higher d's (including the low-energy continuum) expand. These ideas are discussed in more detail elsewhere in connection with Hg.[23] The energy independence of the difference between nonrelativistic and relativistic phase shifts may now be understood in the same manner as for the discrete splitting, but now considering both the spin-orbit interaction and the change in the potential due to interior relativistic contraction.

In Fig. 2, relativistic $d_{3/2}$ phase shifts are shown as a function of atomic number Z; the $d_{5/2}$ results are not shown since, as discussed above, they lie just below and are parallel to the $d_{3/2}$ values. The systematics in Z is exactly the same as the nonrelativistic case[21]; at and just below a noble-gas configuration (Rn, $Z = 86$) there is a slight rise above threshold before the eventual fall, while for higher Z the phase shifts decrease monotonically. A detailed discussion for the nonrelativistic case has been given elsewhere.[21] The s-wave phase shifts, shown in Fig. 3, which we will also need in determing angular distributions, are also very similar to the nonrelativistic cases. However, for the reasons discussed above, the nonrelativistic phase shifts are slightly *less* than the relativistic phase shifts and are parallel to them.
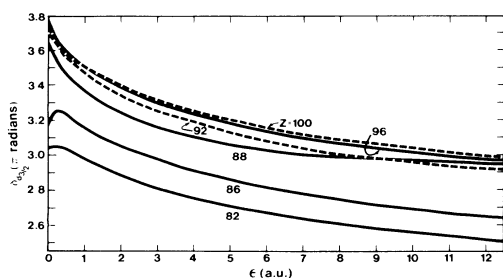

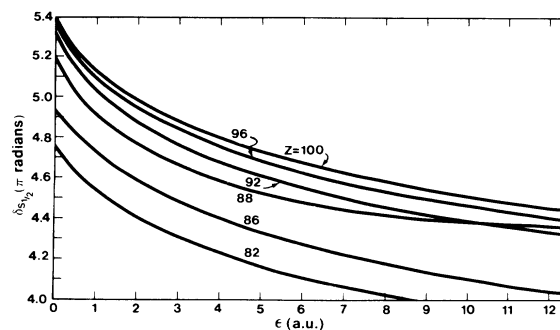FIG. 3. Phase shifts for the $s_{1/2}$ wave for a variety of elements vs photoelectron energy ϵ.

B. Transition matrix elements and cross sections

The cross sections for $6p_{3/2}$ and $6p_{1/2}$ photoionization of U are shown in Fig. 4, plotted versus photon energy. Two imporant features of the energy dependence emerge clearly from this data. First, for both cross sections one may distinguish a near-threshold region of extremely rapid drop with increasing energy and a high-energy region where the falloff is much more gradual. Second, the $6p_{3/2}$ cross section falls off more rapidly than the $6p_{1/2}$ cross section near threshold and then reaches the region of slow decrease at a much lower energy than does the $6p_{1/2}$. Both of these features are due to the existence of zeros in the $p \rightarrow d$ dipole matrix elements, generally referred to as Cooper minima,[5,6] which we will discuss in detail in Sec. III C. The key fact is that the $p_{3/2} \rightarrow d_{3/2}$ and $p_{3/2} \rightarrow d_{5/2}$ minima occur at much lower energy than for $p_{12} \rightarrow d_{3/2}$, a fact indicated by the change of shape of the $6p_{3/2}$ at much lower energy than $6p_{1/2}$.

The reasons for the change in shape of these cross sections can be better understood from Fig. 5, where the cross sections for the individual final-state subchannels

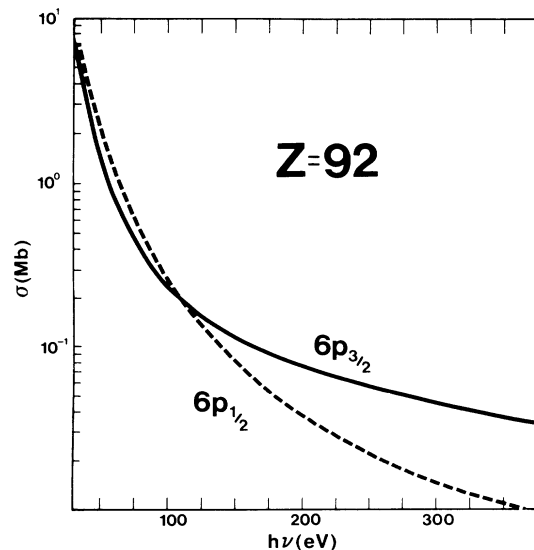FIG. 2. Phase shifts for the $d_{3/2}$ wave for a variety of elements vs photoelectron energy ϵ.

FIG. 4. Photoionization cross sections for $6p_{1/2}$ and $6p_{3/2}$ subshells in uranium.
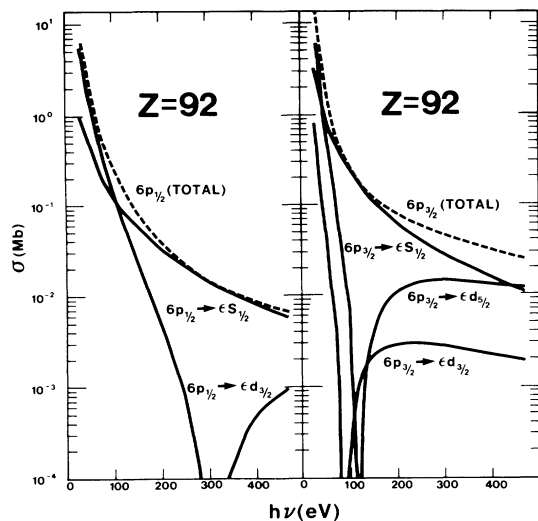
FIG. 5. Photoionization cross sections for $6p_{1/2}$ and $6p_{3/2}$ subshells in uranium. Subshell cross sections are shown with the dashed lines, while the solid lines indicate the contributions of the individual subchannels.

(corresponding to the magnitudes of the transition matrix elements) are shown, along with the totals for U $6p_{1/2}$ and $6p_{3/2}$ photoionization. Looking first at the simpler $6p_{1/2}$ case (where there are only two subchannels) in Fig. 5(a), we see that near threshold the cross section is dominated by the $6p_{1/2} \rightarrow \epsilon d_{3/2}$ transition, which however is rapidly decreasing. In the (200–400) eV range, which brackets the zero (Cooper minimum) at ~ 300 eV in the $6p_{1/2} \rightarrow \epsilon d_{3/2}$ dipole matrix element, and continuing to even higher energies, the dominant contribution is from the more slowly changing $6p_{1/2} \rightarrow \epsilon s_{1/2}$ cross section; the $\epsilon d_{3/2}$ term has not reestablished its dominance even at 500 eV. This shows explicitly the part played by the Cooper minimum in the change of slope of the $6p_{1/2}$ cross section.

The situation for $6p_{3/2}$, shown in Fig. 5(b), is much the same, though slightly more complicated owing to the existence of two $p \rightarrow d$ subchannels, $6p_{3/2} \rightarrow \epsilon d_{3/2}$ and $6p_{3/2} \rightarrow \epsilon d_{5/2}$, each of which has a zero. The cross section is dominated by the $p \rightarrow d$ transitions near threshold, but only for a small energy region. The $p \rightarrow d$ transitions are seen to have zeros in the region of 100 eV, so that in the range 70–150 eV $6p_{3/2} \rightarrow \epsilon s_{1/2}$ dominates the cross section. Above this region the $p \rightarrow d$ transitions again become important, rising to second maxima, but their falloff from these second maxima is very slow, thus continuing the rather shallow falloff of the $6p_{3/2}$ cross section. Thus in the case of $6p_{3/2}$ as well the minima play a crucial role in the overall shape of the cross section.

We note that in addition to the $6p_{1/2}$ minimum being at much higher energy than the $6p_{3/2}$ minima, Fig. 5 also shows that this minimum is much broader. The positions and widths of the minima are related, as we will discuss in Sec. III C.

We further note from Fig. 4 that even though the $6p_{3/2}$ subshell contains four electrons while the $6p_{1/2}$ contains only two, the $6p_{1/2}$ cross section is greater than the $6p_{3/2}$

in the vacuum ultraviolet region. This is, of course, due to the low-energy minima in the $6p_{3/2}$ cross section. At somewhat higher energies, the situation reverses and the $6p_{3/2}$ cross section is more than a factor of 2 larger than the $6p_{1/2}$ owing to the minimum in $6p_{1/2} \rightarrow \epsilon d_{3/2}$ at these energies. This feature will be discussed further in Sec. III D.

We may now examine the Z dependence of these features. In Figs. 6 and 7, respectively, the $6p_{3/2}$ and $6p_{1/2}$ cross sections are shown for a number of elements. (Note that the cross sections are substantially lower for $Z=82$, where there are only two electrons in the $6p$ shell, while in the other cases shown the shell if filled.) It can be seen that our discussion for uranium is, in fact, generally applicable to $6p$ photoionization throughout the range $82 \leq Z \leq 100$ which we have investigated. We note that in Fig. 6 (the $6p_{3/2}$ case) the change of shape, occuring in the energy region of the Cooper minimum, takes place at about the same energy for all Z, indicating that the minima do not change much as a function of Z; at higher energies all of the curves are roughly parallel. However, for the $6p_{1/2}$ cross sections in Fig. 7, the curves are somewhat less parallel and the positions at which they change in shape vary with Z, indicating that the position of the $6p_{1/2}$ minimum is more dependent on Z. For example, the ratio between the $6p_{3/2}$ cross sections for Fm $(Z=100)$ and Rn $(Z=86)$ is almost exactly 2 at the photoelectron energies of both 7 and 14 a.u. while for the $6p_{1/2}$ the ratio is more than 3 at 7 a.u. but slightly less than 2 at 14 a.u.
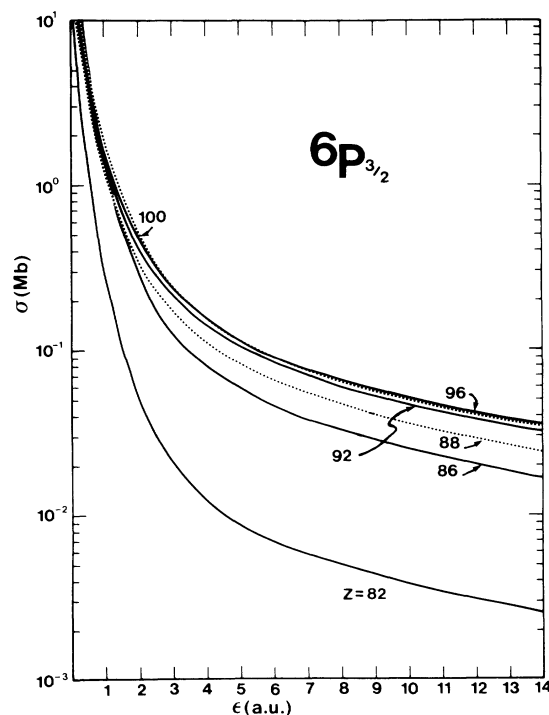

FIG. 6. $6p_{3/2}$ photoionization cross sections for a variety of elements vs photoelectron energy. Note that the cross section for $Z=82$ (Pb) is anomalously small since it has only two electrons in the $6p$ subshell while the other elements have full $6p$ subshells.
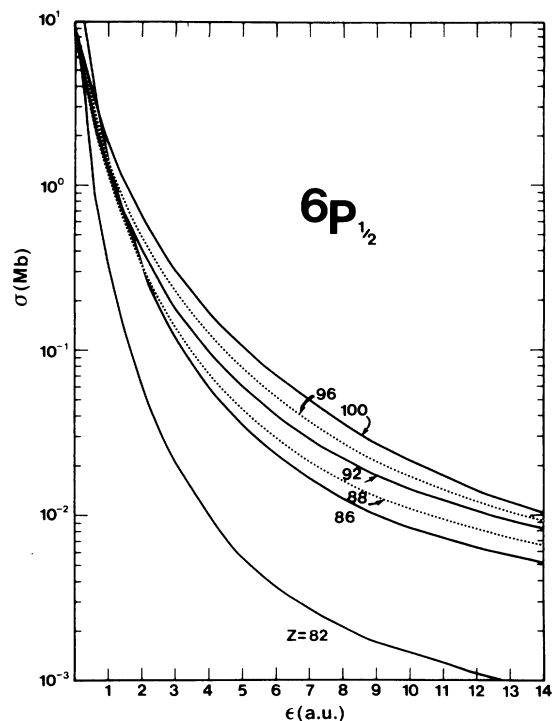
FIG. 7. Same as Fig. 6 for $6p_{1/2}$ photoionization.

FIG. 9. $6p_{1/2}$ photoionization cross sections as in Fig. 7, but with an expanded energy scale showing detail of the threshold region.

The more detailed behavior of these cross sections near threshold is shown in Figs. 8 and 9 for $6p_{3/2}$ and $6p_{1/2}$, respectively. A great deal of variation of the cross sections with Z is evident, which we shall not attempt to discuss in detail at this time. We do note, however, that the most rapid drops with energy are for $Z=82$ and 86 for both $6p_{3/2}$ and $6p_{1/2}$, where more of the oscillator strength is concentrated near threshold. This can be un-
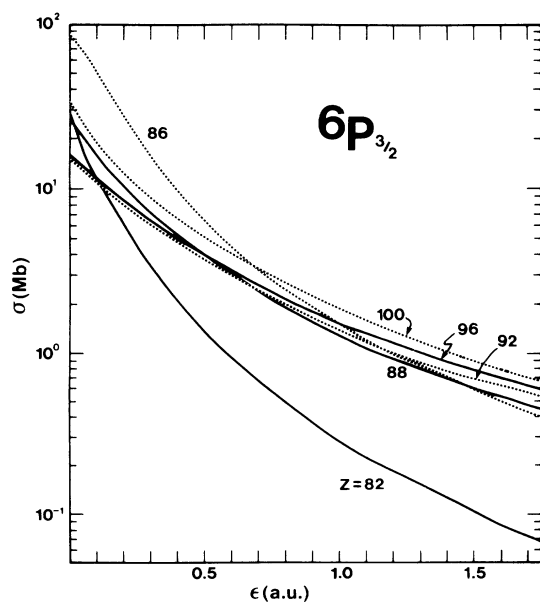

FIG. 8. $6p_{3/2}$ photoionization cross sections as in Fig. 6, but with an expanded energy scale showing detail of the threshold region.
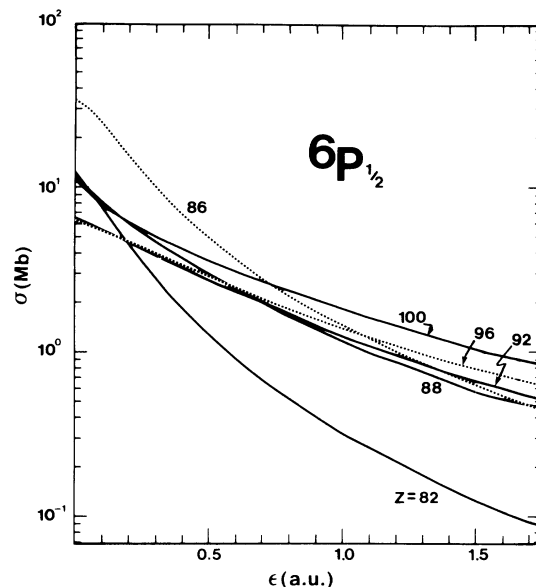
derstood by noting that the cross sections in this region are primarily $p \rightarrow d$ as seen in Fig. 5 for uranium, and that the drop in cross section is a result of the ϵd's moving in toward the nucleus with increasing energy. Thus anything which accelerates this moving in will make the cross section fall still more rapidly. In these two cases the d-wave phase shift is *increasing* from threshold (as shown in Fig. 2) moving the ϵd's inward more rapidly. Thus the energy dependence is accelerated, in these cases, as compared to the others which have d-wave phase-shift energy dependences which *decrease* from threshold. Other correlations between the energy dependence of the cross sections and of the d-wave phase shifts can also be seen; the more rapidly the phase shift decreases, the more slowly the cross section falls with energy in the threshold region.

The total $6p$ subshell cross sections are shown in Fig. 10; these are simply a sum of the $6p_{1/2}$ and $6p_{3/2}$ cross sections discussed above. A selected comparison of these results with nonrelativistic results using the *same* atomic model (which however does *not* mean the *same* potential) is given in Fig. 11. We have verified that the difference between relativistic and nonrelativistic potentials used in the same model calculation (whether relativistic or nonrelativistic) is small. Although the general systematics of the nonrelativistic cross sections is qualitatively similar to the relativistic, two important differences in detail emerge, which have the consequence that nonrelativistic predictions are quantitatively poor throughout the low-energy regime. (This is in contrast to the low-energy region of *inner* shells for which, contrary to one's first expectation, relativistic effects are small.) First, the relativistic cross sections are considerably larger than the nonrelativistic at threshold, owing to the fact that the nonrelativistic d-wave phase shifts are greater than the relativistic (cf. Fig. 1), so that the nonrelativistic d wave is pulled in relative to
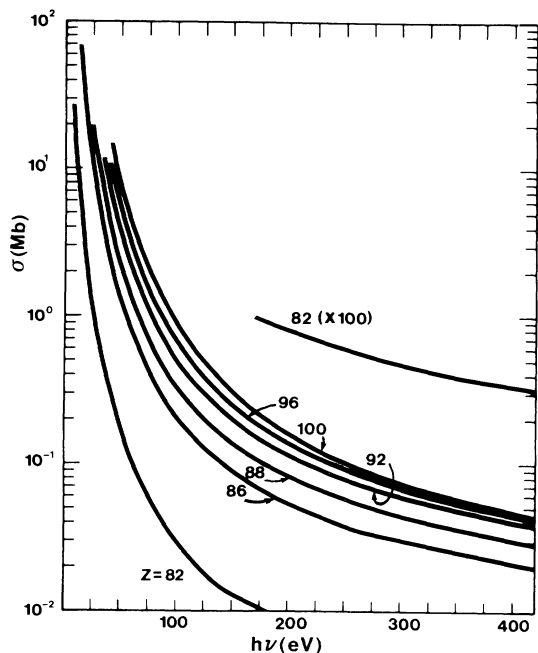
FIG. 10. Total 6p photoionization cross sections for a number of elements.

the relativistic which decreases the matrix element. This is further enhanced by bound-state effects which pull the relativistic 6p's in compared to the nonrelativistic. Second, the change of slope comes at a much lower energy in the nonrelativistic calculation, indicating that the non-relativistic Cooper minima are much lower in energy than the relativistic. In the next section we present a discussion
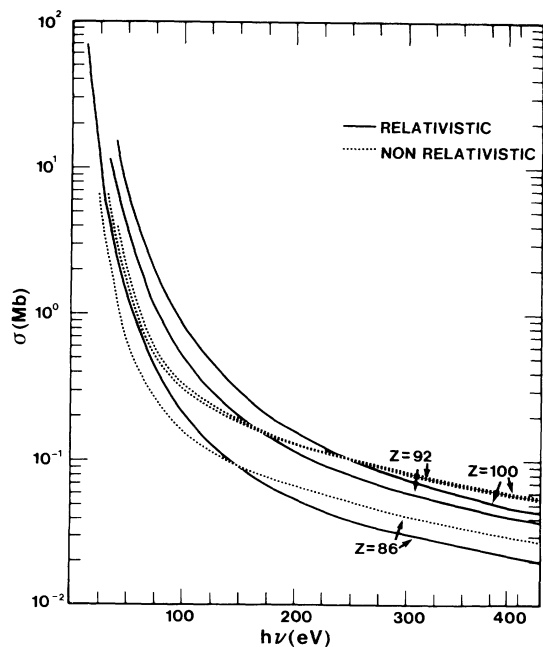

FIG. 11. Comparison of total 6p photoionization cross section in relativistic (Dirac-Slater) and nonrelativistic (Hartree-Slater) approximations for three elements.

of these minima.

Before proceeding to that discussion, it is worthwhile to note that all of the above results are from calculations in the electric dipole approximation; higher multipoles have not been included. We have, in fact, calculated the higher multipoles but their effect on the total cross sections in the energy range we are considering is very minor.

C. Cooper minima

As we discussed previously, the single nonrelativistic $p \rightarrow d$ matrix element is replaced by three separate relativistic matrix elements, each exhibiting a change in sign (Cooper minimum) but at a different photoelectron energy. The trajectory in energy of these minima in the relativistic and nonrelativistic matrix elements, as a function of Z, is shown in Fig. 12. There are several striking features in these results. First, we note the strong Z dependence of the $6p_{1/2} \rightarrow \epsilon d_{3/2}$ minimum. For $Z = 82$ it is located about 200 eV above threshold, while by $Z = 100$ it appears about 460 eV above. Second, the energy splitting between the $6p_{3/2}$ minima and the $6p_{1/2}$ is huge, being 100 eV for $Z = 82$ and increasing to more than 300 eV by $Z = 100$. There is also a splitting between the $6p_{3/2} \rightarrow \epsilon d_{3/2}$ and $6p_{3/2} \rightarrow \epsilon d_{5/2}$ minima which increases slowly from about 20 eV at $Z = 82$ to almost 50 eV at $Z = 100$, as can be seen from Fig. 12. Further, the locus of the nonrelativistic $p \rightarrow d$ minima lies below any of the relativistic minima, roughly a constant 10 eV below the $p_{3/2} \rightarrow d_{3/2}$ minima independent of Z. Thus the effect of relativistic interactions is both to move the minima to higher energy and to introduce a very significant energy splitting among them.

To understand these results, consider first the $p_{1/2} \rightarrow d_{3/2}$ and $p_{3/2} \rightarrow d_{3/2}$ minima. In our DS calculation for a given photoelectron energy ϵ, the $\epsilon d_{3/2}$ wave function is exactly the same, independent of the initial state of the photoelectron. Thus since the final state in each of these transitions is exactly the same, the huge splitting must result from the differences between the $6p_{1/2}$ and $6p_{3/2}$ bound-state wave functions. In first ap-
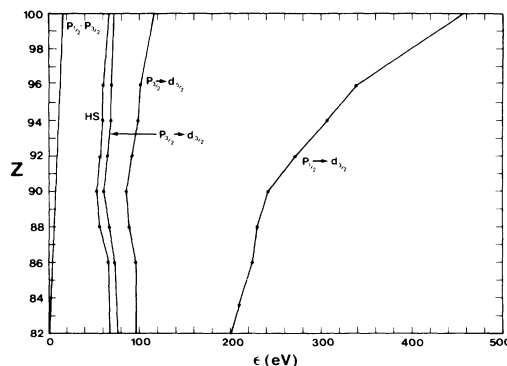

FIG. 12. Trajectory (in photoelectron energy) of the "Cooper" zeros in the $6p \rightarrow d$ dipole matrix elements, as a function of Z. Various relativistic matrix elements are labeled, while HS refers to the nonrelativistic Hartree-Slater results. Also shown, for comparison, is the spin-orbit splitting of the $6p_{1/2}$-$6p_{3/2}$ energy levels as a function of Z.

proximation, in regions where these wave functions are large, the $6p_{1/2}$ wave function is the same as the $6p_{3/2}$ only displaced inward towards the nucleus, because the spin-orbit force is attractive for $j = l - \frac{1}{2}$ but repulsive for $j = l + \frac{1}{2}$. Thus at the energy for which the overlap of the $6p_{3/2}$ wave function is such that the dipole matrix element vanishes, the radial extent of the $\epsilon d_{3/2}$ is still too great to have the similar overlap needed for the $6p_{1/2}$ matrix element to vanish. Since continuum wave functions move *in* with increasing energy, it is clear that the $6p_{1/2}$ minimum will occur at a higher energy.

The $6p_{1/2} \rightarrow 6p_{3/2}$ spin-orbit splitting of bound-state energies, also shown in Fig. 12, is an order of magnitude smaller than the splitting of the minima. One might think that the same energy difference by which the discrete $p_{1/2}$ is displaced inward from the $p_{3/2}$ should cause the $\epsilon d_{3/2}$ to move in similarly, so that the minima would be split by about the same amount as the discrete states. This is not true, owing to the centrifugal barrier for d waves which makes it far more difficult for continuum d waves to penetrate the core region than the discrete p orbitals. The strength of the centrifugal barrier for d waves, then, is responsible for the more than tenfold "magnification" of the splitting, while the increasing strength of the spin-orbit interaction as Z increases causes the increased splitting of the minima with Z.

We see from Fig. 12 that the location of the $6p_{3/2} \rightarrow \epsilon d_{3/2}$ zero varies little with Z, while as already noted the $6p_{1/2} \rightarrow \epsilon d_{3/2}$ shows an extremely strong variation. In examining this difference, we have observed that both $6p$ wave functions move in about the same amount with increasing Z; the displacement of $6p_{1/2}$ inward with respect to $6p_{3/2}$ remaining roughly constant. (Although the $6p_{1/2} \rightarrow 6p_{3/2}$ spin-orbit energy splitting increases with increasing Z, it also takes a larger energy to displace the wave functions as they move toward the interior of the atoms where the potential is larger.) The d wave functions are also displaced inward with increasing Z, and just enough so that the $6p_{3/2} \rightarrow \epsilon d_{3/2}$ minimum has very little variation with Z. Then, although the $\epsilon d_{3/2}$ wave function moves in the same *distance* for each Z to get to the point where the $6p_{1/2} \rightarrow \epsilon d_{3/2}$ matrix element vanishes, since the $6p$'s are displaced inward with increasing Z it takes more and more energy for the $\epsilon d_{3/2}$ to move in that distance owing to the strength of the d-wave potential barrier. Thus a given energy increase has a greater effect on the $\epsilon d_{3/2}$ wave function in the vicinity of the $6p_{3/2}$ minimum than near the $6p_{1/2}$ minimum, which occurs when the continuum wave function is closer in. This is the reason that the $6p_{1/2}$ minimum is so much wider than those of $6p_{3/2}$, as shown in Fig. 5.

The much smaller splitting between the $6p_{3/2} \rightarrow \epsilon d_{3/2}$ and $6p_{3/2} \rightarrow \epsilon d_{5/2}$ minima is evidently due to the final continuum states, since the initial states are exactly the same. The spin-orbit force pulls the $\epsilon d_{3/2}$ in and pushes the $\epsilon d_{5/2}$ out; thus the $\epsilon d_{3/2}$ minimum occurs at lower energy, as seen in Fig. 12. In addition, the increase in the strength of the spin-orbit interaction with Z causes the increase in the separation of this minima with Z.

Finally, we note that the nonrelativistic $6p \rightarrow \epsilon d$ minimum behaves almost exactly like the $6p_{3/2} \rightarrow \epsilon d_{3/2}$

minimum, as a function of Z. Owing to the relativistic contraction of the core, the electrostatic attraction becomes greater for p states and less for d states, as compared to nonrelativistic, as discussed in Sec. III A. But, the $6p_{3/2}$ also "feels" a spin-orbit repulsion makes its *net* attraction similar to nonrelativistic, while the $\epsilon d_{3/2}$ "feels" a spin-orbit attraction, so its *net* attraction is also close to nonrelativistic.

D. Branching ratios

The $6p_{3/2}:6p_{1/2}$ branching ratios are shown in Fig. 13. A strong energy dependence is seen in all cases, along with a very significant deviation from the nonrelativistic (statistical) ratio of 2. Just above threshold, all of the branching ratios are less than one. At higher energies, all of the branching ratios increase dramatically, the amount of the increase becoming greater with Z. At still higher energies they will once again drop.

These results can be understood very simply from our discussion of the Cooper minima. The very low values for the branching ratios just below 100 eV are a consequence of the fact that the $6p_{3/2}$ cross sections are anomalously low due to their Cooper minima. The minima in the branching ratios move to slightly higher energies with increasing Z because the $6p_{3/2}$ Cooper minima move out slightly with increasing Z (cf. Fig. 12). The minimum values of the branching ratios decrease (less than 0.5 for $Z = 100$) with increasing Z (note that the $6p_{1/2}$ cross section is larger for these energies in the higher Z's since its Cooper minimum has moved out very far from this energy region). At higher energies the situation reverses, for now the $6p_{1/2}$ cross sections have Cooper minima while the $6p_{3/2}$ cross sections have "recovered." Since the $6p_{1/2}$ Cooper minima move out so dramatically with increasing Z, the curves in the higher-energy region differ widely with Z. Evidently (neglecting other energy variations of the cross sections) the further out the $6p_{1/2}$ Cooper minimum, the more the $6p_{3/2}$ cross section will have "recovered," and so the larger the branching ratio, as observed for increasing Z.

For the lower Z's our calculations have been done at sufficiently high energies that the branching ratios have flattened out and begun to decrease. We may expect the
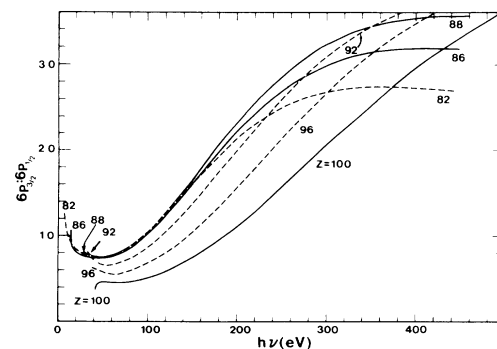

FIG. 13. $6p_{3/2}:6p_{1/2}$ photoionization branching ratios for a number of elements. Note that these are plotted against *photon* energy.

same behavior for the higher Z's, albeit at higher energies, as has been shown in our work for U.[10] (For light Z, but not heavy Z, there is ultimately still another rise in the branching ratio at mc^2 energies.) The slow variation with energy at these higher energies reflects the lack of structure, whether Cooper minima or shape resonances, in the matrix elements.

E. Photoelectron angular distributions

The photoelectron angular distribution asymmetry parameter β is shown in Fig. 14 for six Z's; the $6p_{3/2}$, $6p_{1/2}$, and nonrelativistic $6p$ values are shown in each case. All the curves have the same general shape—a rapid rise from threshold to a maximum of close to 2 followed by a descent to a minimum and a subsequent gradual rise. The outstanding feature of these results is the significant difference between the β's for the $6p_{1/2}$ and $6p_{3/2}$ cases, a difference which increases markedly with increasing Z. These features are not due to the behavior of the phase shifts, which vary smoothly and steadily with energy, but to the matrix elements.

To understand these results we may begin by noting that, from Eq. (6), at the energy of the $6p_{1/2} \rightarrow \epsilon d_{3/2}$ Cooper minimum where $R_{d_{3/2}}$ vanishes, $\beta_{6p_{1/2}}$ is zero as well. This occurs in the descent of the β's from their maxima near threshold; since the Cooper minima move out in energy with Z, the $6p_{1/2}$ β curves also move out, as is seen in Fig. 14.

The structure of $\beta_{6p_{3/2}}$, given in Eq. (7) is somewhat more complicated than $\beta_{6p_{1/2}}$ owing to the fact that $\beta_{6p_{3/2}}$ is expressed in terms of dipole matrix elements with both the $\epsilon d_{3/2}$ and the $\epsilon d_{5/2}$ channel. Nevertheless, owing to angular factors, it is seen from Eq. (7) that the $\epsilon d_{5/2}$ channel dominates and $\beta_{6p_{3/2}}$ goes to zero very close to the $6p_{3/2} \rightarrow \epsilon d_{5/2}$ Cooper minimum; the $6p_{3/2} \rightarrow \epsilon d_{3/2}$ channel acts as a small perturbation. Since the $d_{5/2}$ minimum moves only slowly with Z (and the $d_{3/2}$ minima does not

move), $\beta_{6p_{3/2}}$ remains roughly the same, moving out only a little with increasing Z. Thus the $6p_{3/2}$ β's do not change appreciably as a function of Z, while those of the $6p_{1/2}$ cases move out significantly.

The nonrelativistic[24] β's show features similar to the $6p_{3/2}$ case, but correspond to lower energies, owing to the fact that the nonrelativistic Cooper minima are at lower energies than the relativistic. The rather good agreement of all of the results, for each Z at threshold and just above is a consequence of the facts that their behavior depends primarily upon the rapid variation of the low-energy Coulomb phase shifts,[24] which are virtually unaffected by relativity, and the threshold phase shifts, which are only weakly perturbed by relativistic interactions.

The effect of higher multipoles on the photoelectron angular distribution has not been considered in the foregoing discussion. Higher multipoles can affect β itself,[25,10] as well as change the form of Eq. (5), which is only true for electric dipole radiation.[11] The general form of the photoelectron angular distribution from an unpolarized photon beam is[11,16]

$$\frac{d\sigma}{d\Omega} = \frac{\sigma}{4\pi} \sum_{n=0}^{\alpha} B_n P_n(\cos\theta) , \qquad (8)$$

where all of the B_n reduce to zero in the dipole approximation except $B_0 = 1$, and B_2 which then is $-\frac{1}{2}\beta$ as described above. In the energy range considered in this work, $h\nu \lesssim 500$ eV, previous work on the uranium[10] has shown that the only nondipole terms giving a nonnegligible contribution in Eq. (8) are B_1 and B_3; their contributions are about 5% and so may need to be considered in comparisons with experiment. Nondipole contributions to B_2 (i.e., to β of this paper) are negligible except in the vicinity of a deep Cooper minimum. (For similar reasons, at these energies higher multipole effects on total cross sections or on branching ratios are also normally negligible.)

IV. FINAL REMARKS

In summary then, we have found that relativistic effects introduce very dramatic shifts and splittings of the $6p \rightarrow \epsilon d$ Cooper minima. The $6p_{3/2}$ Cooper minima are much closer to threshold than the $6p_{1/2}$ minima. In consequence, the $6p_{3/2}$:$6p_{1/2}$ branching ratios are very strongly energy dependent, being very low (less than unity) in the near-threshold region and rising to rather large values (~ 3 or greater) for higher energies. In addition, the splittings of the Cooper minima lead to significant differences in the photoelectron angular distribution asymmetry parameter β between the $6p_{1/2}$ and $6p_{3/2}$ cases. The total $6p$ subshell cross sections are not affected by the relativistic interactions nearly as much as the angular distributions or branching ratios.

Unfortunately, there is almost no experimental data on $6p$ photoionization [except for some He I photoelectron data for Tl,[26] Bi,[27] and Pb (Ref. 17)] so we cannot assess our calculated results in comparison with experiment. It is important to realize that the inclusion of correlation and full exchange in the initial- and final-state wave func-
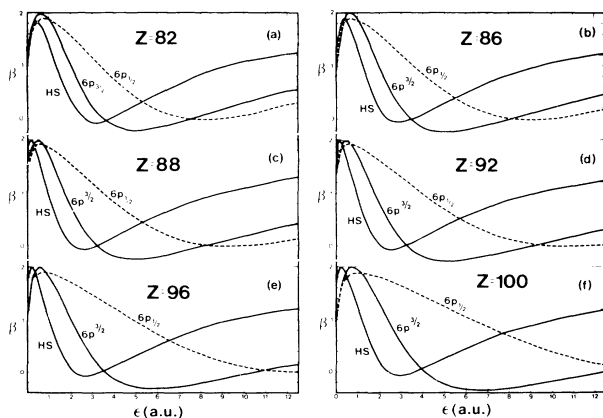

FIG. 14. Photoelectron angular distribution asymmetry (β) parameters for the $6p$ subshells in six elements, shown vs photoelectron energy, ϵ. In each curve the relativistic $6p_{3/2}$ and $6p_{1/2}$ results are given along with the nonrelativistic Hartree-Slater (HS) result.

tions will modify these results quantitatively. However, it is highly unlikely that more sophisticated treatments will alter our conclusions qualitatively. In fact, some parallel work using the far more sophisticated relativistic random-phase approximation for Rn and Ra has indicated that the results presented in this paper are substantially correct insofar as the splitting of the minima and the systematics of the branching ratios and β's are concerned.[28]

Nevertheless, the need for experimental work, difficult though it may be with such targets, is clear.

ACKNOWLEDGMENTS

[*]Permanent address: Racah Institute of Physics, Hebrew University of Jerusalem, Jerusalem 91904, Israel.

[1]U. Fano and J. Cooper, Rev. Mod. Phys. 40, 441 (1968).

[2]S. T. Manson, Adv. Electron. Electron Phys. 41, 73 (1976); 44, 1 (1977).

[3]Photoionization and Other Probes of Many-Electron Interactions, edited by F. J. Wuilleumier (Plenum, New York, 1976).

[4]A. F. Starace, in Handbuch der Physik, edited by W. Mehlhorn (Springer, Berlin, 1981), Vol. 31, pp. 1-121.

[5]J. W. Cooper, Phys. Rev. 128, 681 (1962).

[6]S. T. Manson and J. W. Cooper, Phys. Rev. 165, 126 (1968).

[7]Y. S. Kim, A. Ron, R. H. Pratt, B. R. Tambe, and S. T. Manson, Phys. Rev. Lett. 46, 1326 (1981).

[8]T. E. H. Walker and J. T. Waber, J. Phys. B 6, 1165 (1973).

[9]W. Ong and S. T. Manson, Phys. Rev. A 20, 2364 (1979).

[10]Y. S. Kim, R. H. Pratt, A. Ron, and H. K. Tseng, Phys. Rev. A 22, 567 (1980).

[11]C. N. Yang, Phys. Rev. 74, 764 (1948).

[12]J. Cooper and R. N. Zare, in Lectures in Theoretical Physics, edited by S. Geltman, K. Mahanthappa, and W. Britten (Gordon and Breach, New York, 1969), Vol. II C, pp. 317-337.

[13]J. W. Cooper and S. T. Manson, Phys. Rev. 177, 157 (1969).

[14]D. Lieberman, D. T. Cromer, and J. T. Waber, Comput. Phys. Commun. 2, 107 (1971).

[15]W. Ong and S. T. Manson, Phys. Rev. A 19, 688 (1979).

[16]R. H. Pratt, A. Ron, and H. K. Tseng, Rev. Mod. Phys. 45, 273 (1973).

[17]S. Süzer, M. S. Banna, and D. A. Shirely, J. Chem. Phys. 63, 3473 (1975).

[18]J. H. Scofield, Phys. Rev. 179, 9 (1969).

[19]J. H. Scofield, Lawrence Livermore Laboratory Report No. UCRL-51326 (unpublished).

[20]D. J. Kennedy and S. T. Manson, Phys. Rev. A 5, 227 (1972).

[21]S. T. Manson, Phys. Rev. 182, 97 (1969).

[22]H. A. Bethe and E. E. Salpeter, Quantum Mechanics of One- and Two- Electron Atoms (Springer, Berlin, 1957), pp. 22, 72.

[23]J. P. Desclaux and Y.-K. Kim, J. Phys. B 8, 1177 (1975).

[24]S. T. Manson, J. Electron Spectrosc. 1, 413 (1973).

[25]H. K. Tseng, R. H. Pratt, Simon Yu, and Akiva Ron, Phys. Rev. A 17, 1061 (1978).

[26]S. Süzer, Chem. Phys. Lett. 69, 230 (1980).

[27]S. Süzer S.-T. Lee, and D. A. Shirely, J. Chem. Phys. 65, 412 (1976).

[28]V. Radójevic, P. Deshmukh, and S. T. Manson, Bull. Am. Phys. Soc. 28, 814 (1983).